ACS Photonics

Article

Cite This: ACS Photonics 2019, 6, 1681−1689

pubs.acs.org/journal/apchd5

# Organic Monolithic Natural Hyperbolic Material

Yeon Ui Lee,[†] Olivier P. M. Gaudin,[‡] KwangJin Lee,[†] Eunyoung Choi,[▽] Virginie Placide,[†] Kazuto Takaishi,[§,∥] Tsuyoshi Muto,[§] Pascal André,[§,⊥] Atsuya Muranaka,[§] Masanobu Uchiyama,[§,#] Fabrice Mathevet,[¶] Tetsuya Aoyama,[§] JeongWeon Wu,*[,†,▽] Anthony D'Aléo,*[,†,□,△,▽] and Jean-Charles Ribierre*[,⬡]

[†]Department of Physics, Ewha Womans University, Seoul 03760, Republic of Korea

[‡]Thorn Lighting Limited, House of Light, Butchers Race, Green Lane Industrial Estate, Spennymoor, Co. Durham DL16 6HL, United Kingdom

[§]Elements Chemistry Laboratory, RIKEN Cluster for Pioneering Research (CPR), 2-1 Hirosawa, Wako 351-0198, Japan

[∥]Division of Applied Chemistry, Graduate School of Natural Science and Technology, Okayama University, Tsushima, Okayama 700-8530, Japan

[⊥]School of Physics and Astronomy, University of St Andrews, North Haugh, St Andrews KY16 9SS, United Kingdom

[#]Graduate School of Pharmaceutical Sciences, The University of Tokyo, 7-3-1 Hongo, Bunkyo-ku, Tokyo 113-0033, Japan

[¶]Sorbonne Université, Faculté des Sciences, CNRS, Institut Parisien de Chimie Moléculaire (IPCM), UMR 8232, Chimie des Polymères, 4 Place Jussieu, 75005 Paris, France

[□]Building Blocks for Future Electronics Laboratory (2-B FUEL), The joint CNRS-Ewha-Yonsei Laboratory, UMI 2002, Seoul, Republic of Korea

[△]Aix Marseille Université, CNRS, CINaM UMR 7325, Campus de Luminy, Case 913, 13288 Marseille, France

[▽]Center for Quantum Nanoscience, Institute for Basic Science, Seoul 03760, Republic of Korea

[⬡]State Key Laboratory of Modern Optical Instrumentation, College of Optical Science and Engineering, Zhejiang University, Hangzhou 310027, China

Supporting Information

**ABSTRACT:** Materials with hyperbolic dispersion are the key to a variety of photonic applications involving nanoimaging, hyper-lensing, and spontaneous emission engineering, due to the availability of high $k$ modes. Here we demonstrate that spin-coated polycrystalline organic semiconducting films with a layered molecular packing structure can exhibit a hyperbolic dispersion over a wide spectral range and support the presence of surface excitonic polaritons. This was evidenced from 670 to 920 nm and is related to the negative real part of the dielectric permittivity of the selected quinoidal organic semiconductor. In addition, the accessible high $k$ modes lead to changes in the spontaneous emission decay rate and photoluminescence quantum yield of emitters placed nearby the organic monolithic (composed of only one molecule and not necessitating an alternating multilayer structure) natural hyperbolic material. This study opens a new route toward single-step solution manufacturing of large-area, low-cost, and flexible organic photonic metadevices with hyperbolic dispersion.

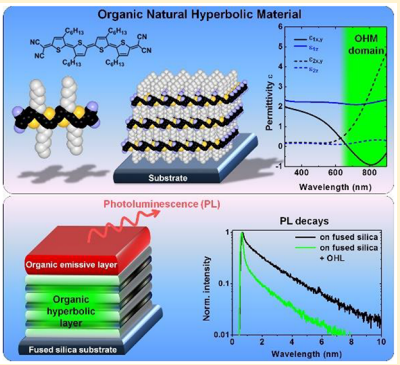


**KEYWORDS:** *organic natural hyperbolic material, organic semiconductor, layered molecular packing structure, surface excitonic polaritons, spontaneous emission engineering*

Uniaxial anisotropic materials with in-plane and out-of-plane components of the real part of the permittivity possessing opposite signs are referred to as hyperbolic media. Metallic nanowire arrays and metal−dielectric multilayers are two well-known examples of such hyperbolic metamaterials (HMMs).[1] These anisotropic structured materials show unusual light propagation and remarkable optical properties including negative refraction and subwavelength imaging and focusing.[2] In addition, the accessible high wave-vector ($k$) spatial modes of the HMMs strongly modify the local density of states (LDOS), resulting in an enhancement of the spontaneous emission rate of emitters placed nearby HMMs.[3] Importantly, this effect can take place at any desired wavelength due to the tunable dispersion relation of HMMs and the broadband singularity in the LDOS.[4] These features

**Received:** January 31, 2019
**Published:** May 13, 2019






DOI: 10.1021/acsphotonics.9b00185
ACS Photonics 2019, 6, 1681−1689

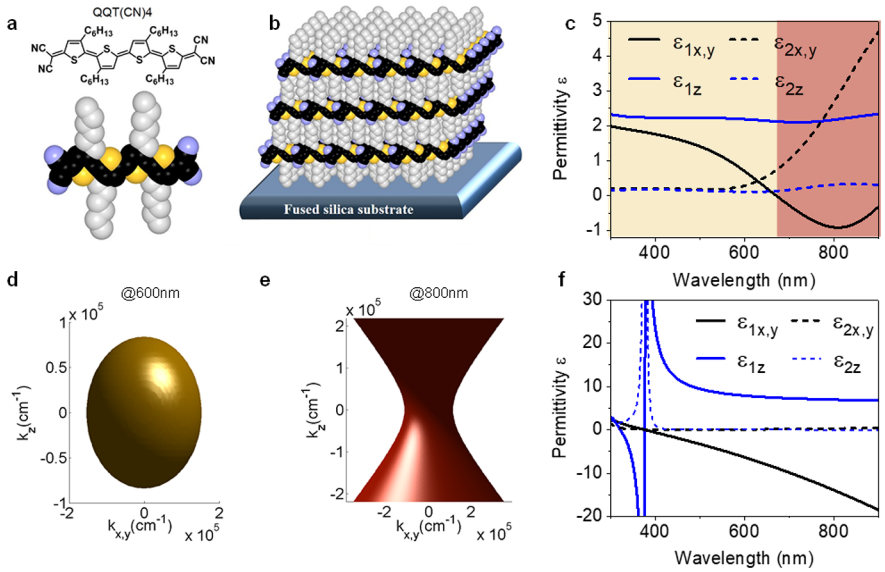


**Figure 1.** (a) Molecular structure and space-filling representation of QQT(CN)4 (insulating alkyl side chains are represented in gray). (b) Schematic representation of the layered molecular packing structure in spin-coated polycrystalline QQT(CN)4 thin films. (c) *x,y* component and *z* component of the real and imaginary parts of the complex permittivity of QQT(CN)4. (d, e) Isofrequency contour showing that the QQT(CN)4 film behaves as an elliptic and an hyperbolic medium at 600 and 800 nm, respectively. (f) *x,y* component and *z* component of the real and imaginary parts of the complex permittivity of the $Ag/Al_2O_3$ HMM (fill factor = 0.5).

make HMMs potentially attractive for applications in biosensing, optoelectronic, and light-emitting devices.[5] However, most HMM nanostructures used so far contain metallic components and are fabricated by multiple-step processes. In this context, an important challenge for the photonic industry is the development of novel HMMs that can be prepared in one single step using simple solution-processing methods.[6]

Hyperbolic dispersion has been observed in a variety of natural materials including magnesium diboride, graphite, hexagonal boron nitride, tetradymites, cuprates, ruthenates, sapphire, bismuth, triglycine, perovskites, and calcite.[7] Noticeably, some of these natural hyperbolic materials such as tetradymites and magnesium diboride exhibit a uniaxial optical anisotropy, which is due to their layered structures made of atomic monolayer sequences. Importantly, while the highest $k$ accessible in artificial metallic/dielectric HMMs is determined by the Fourier transform of the minimum of the subwavelength nanostructure size, the largest $k$ in natural hyperbolic materials is only limited by the atomic spacing.[7c] Looking at the natural hyperbolic materials for visible wavelengths, it is worth noting that tetradymites have shown hyperbolic dispersion in the visible and near-infrared spectral range ($300 \leq \lambda \leq 1180$ nm).[8] Nevertheless, they exhibit a relatively large imaginary part of the permittivity ($4 \leq \mathrm{Im}(\varepsilon_{x,y}) \leq 78$, $0 \leq \mathrm{Im}(\varepsilon_z) \leq 53$), leading to high optical losses. Noticeably, gallium telluride has also shown hyperbolic dispersion in the ultraviolet and visible spectral range ($150 \leq \lambda \leq 498$ nm) and relatively large imaginary part of the permittivity ($0 \leq \mathrm{Im}(\varepsilon_x) \leq 10$, $0 \leq \mathrm{Im}(\varepsilon_y) \leq 40$, $0 \leq \mathrm{Im}(\varepsilon_z) \leq 18$).[8] Note that the subscripts ($x$, $y$) and $z$ indicate here the in-plane and out-of-plane components, respectively. In this context, while natural hyperbolic materials clearly provide a promising alternative to artificial metal−dielectric HMMs, further work is still needed to unlock their full potential for photonic applications. Following those requirements, a recent theoretical work using first-principles calculations suggested that other layered compounds such as transition metal dichalcogenides could be attractive for natural hyperbolic materials at optical frequencies.[9]

In this article, we demonstrate that spin-coated organic thin films based on the quinoidal oligothiophene derivative (QQT(CN)4) (see its chemical structure in Figure 1a) exhibit hyperbolic dispersion over a wide spectral range from 670 to 920 nm with real ($-1 \leq \mathrm{Re}(\varepsilon_{x,y}) \leq 0$, $\mathrm{Re}(\varepsilon_z) \sim 2.2$) and imaginary ($0 \leq \mathrm{Im}(\varepsilon_{x,y}) \leq 5$, $0 \leq \mathrm{Im}(\varepsilon_z) \leq 0.5$) parts of the permittivity. The modification of the LDOS in the hyperbolic spectral range is associated with the presence of surface excitonic polaritons (SEPs) in the layered QQT(CN)4 molecular crystalline structure. In addition, the high $k$ modes accessible in this organic monolithic natural hyperbolic material lead to substantial changes in the spontaneous emission decay rate and photoluminescence quantum yield (PLQY) of emitters located nearby the QQT(CN)4 films. To the best of our knowledge, this is the first demonstration of such a SEP effect on the photophysical properties of light-emitting molecules. This study provides evidence that organic monolithic natural hyperbolic materials can offer a promising platform to tailor Purcell factors for any specific emitters. Considering the advantages of organic materials in terms of low cost and easy processing, mechanical flexibility, and chemical tunability, this study opens new perspectives for the molecular-scale design of natural hyperbolic materials and their nanophotonic applications.

Quinoidal oligothiophene derivatives are a well-established class of low-bandgap organic semiconductors for n-type and ambipolar organic field-effect transistors.[10] Among them, the QQT(CN)4 molecule used in this study is composed of a quaterthiophene backbone terminated at both extremities by dicyanomethylene groups.[11] Such a molecular architecture allows the stabilization of the quinoidal form of the quaterthiophene core with a highest occupied molecular orbital (HOMO)−lowest unoccupied molecular orbital (LUMO) bandgap as low as 0.9 eV in thin films.[12] In addition, QQT(CN)4 thin films are simply prepared by spin-


DOI: 10.1021/acsphotonics.9b00185
ACS Photonics 2019, 6, 1681−1689

coating from a chloroform solution and have been found to be highly stable even in the presence of oxygen, making this compound ideally suited for a broad range of experimental studies and applications.[11,12]

The structural properties of spin-coated polycrystalline QQT(CN)4 thin films have been previously investigated by two-dimensional (2D) grazing incident X-ray scattering (GIXS) and atomic force microscopy (AFM). A schematic representation of the molecular packing in the QQT(CN)4 layer is displayed in Figure 1b. The extensive X-ray and AFM experiments carried out in QQT(CN)4 thin films[11−13] demonstrated that (i) this compound self-assembles in a triclinic $P\bar{1}$ unit cell, (ii) the $c^*$ axis of the organic crystals is preferentially oriented in the direction parallel to the substrate normal, (iii) the molecules adopt an edge-on orientation with the molecular lamellae aligning parallel to the substrate plane, (iv) the insulating alkyl side chains of QQT(CN)4 molecules are oriented in the direction perpendicular to the substrate and self-organize in between each molecular layer of quinoidal quaterthiophene backbones, and (v) the spin-coated QQT-(CN)4 films are polycrystalline with an average size of the crystallites in the range between 12 and 40 nm.[12,13b] Such a layered molecular packing with an interplanar $d$-spacing of 14.2 Å was found to be well-adapted for ambipolar charge transport in transistor configuration.[12] As shown in previous works, the HOMO and LUMO levels of QQT(CN)4, the suitable choice of the electrode contact materials, and the influence of the molecular packing on its HOMO and LUMO splittings play indeed a key role on the ambipolar transport properties of the QQT(CN)4 OFETs. The optimized morphology of QQT-(CN)4 can lead to hole and electron field-effect mobilities as high as 0.4 and 0.5 $cm^2\ V^{-1}\ s^{-1}$, respectively.[12] In addition, a previous report has also examined singlet−singlet exciton annihilation and singlet exciton diffusion processes taking place in QQT(CN)4 thin films.[13a] The 1D exciton diffusion model used to describe the experimental results indicated that the singlet excitons migrate in each molecular layer of the QQT(CN)4 backbones preferentially along the $\pi-\pi$ stacking direction with a diffusion length of about 4 nm.

The spectral absorptance of a QQT(CN)4 film and its transmission and reflection spectra are displayed in Figure S1. The organic film shows an intense and broad absorption spanning from the far red to the near-infrared region of the spectrum. Such a broad absorption feature in the solid state has been previously attributed to a strong aggregation of the QQT(CN)4 backbones in each lamella.[12,14] This is confirmed by the semiempirical Hartree−Fock-based Zerner's intermediate neglect of differential overlap/spectroscopy (ZINDO/S) calculations described in Figure S2, showing the important role played by intermolecular interactions on the optical properties of QQT(CN)4 films. The direction of the absorption transition dipole of the QQT(CN)4 molecule was also determined by quantum chemistry calculations and found to be parallel to the long molecular axis. Considering the structural anisotropy of the organic films and the direction of the absorption transition dipole moment, QQT(CN)4 films are expected to show a strong uniaxial optical anisotropy.

Variable angle spectroscopic ellipsometry (VASE) measurements were carried out to determine the optical constants and the dielectric permittivity of QQT(CN4) films. Details about the method, experimental ellipsometry data, and their modeling can be found in the Supporting Information (experimental section and Figures S3−S6). Regarding the uniqueness of the fit of our ellipsometry data, it should be emphasized that a multisample analysis was carried out, using a combination of both $Si/SiO_2$ and fused silica substrates. Such a procedure significantly improves the robustness of the data analysis and was used to make sure that no other model could fit the ellipsometry experimental data. The important insight obtained from the results shown in Figure 1c are (i) the organic films present a strong uniaxial optical anisotropy with an optical axis being oriented normal to the film plane, (ii) nearly no out-of-plane absorption is observed, which is fully consistent with the layered molecular packing structure and the molecular orientation of QQT(CN)4 dyes in thin films, and (iii) the real part of the in-plane permittivity is found to be negative between 670 and 920 nm, while the real part of the out-of-plane permittivity is positive in this spectral range. It should also be mentioned that the morphology of the QQT(CN)4 films and their optical properties are highly stable over several months. In addition, the ellipsometry data were found to be highly reproducible from sample to sample.

The dispersion relation for uniaxial anisotropic materials can be described by

$$\varepsilon_{x,y}^{-1}k_z^2 + \varepsilon_z^{-1}(k_x^2 + k_y^2) = (\omega/c)^2 \quad (1)$$

where $\varepsilon_{x,y} = \varepsilon_x = \varepsilon_y$ is the in-plane complex permittivity and $\varepsilon_z$ is the out-of-plane complex permittivity. Based on the measured complex permittivity dispersion shown in Figure 1c, the equifrequency contour in the wave vector plane gives an ellipsoid shape at a wavelength of 600 nm due to both positive values of $\mathrm{Re}(\varepsilon_{x,y}) = \mathrm{Re}(\varepsilon_x) = \mathrm{Re}(\varepsilon_y)$ and $\mathrm{Re}(\varepsilon_z)$. In contrast, due to the opposite signs of $\mathrm{Re}(\varepsilon_{x,y})$ and $\mathrm{Re}(\varepsilon_z)$, i.e., $\mathrm{Re}(\varepsilon_{x,y}) < 0$, $\mathrm{Re}(\varepsilon_z) > 0$, between 670 and 920 nm, the equifrequency contour shows an hyperboloid shape, indicating that QQT-(CN)4 films undoubtedly exhibit a hyperbolic dispersion in this spectral range. This implies that QQT(CN)4 films should allow the propagation of waves with very large $k$ (only limited by the 14.2 Å spacing between molecular layers). For comparison, the complex refractive index and permittivity of a 4 pair Ag (10 nm)/$Al_2O_3$ (10 nm) HMM and its equifrequency contour are displayed in Figures S7 and S8. It can also be seen from the results displayed in Figure 1c that $0.5 \leq \mathrm{Im}(\varepsilon_{x,y}) \leq 5$ and $0.3 \leq \mathrm{Im}(\varepsilon_z) \leq 0.1$ in the hyperbolic spectral region of QQT(CN)4. While such values of the imaginary part of the permittivity should cause some optical losses, it is interesting to note that they are significantly lower than those reported in other natural hyperbolic materials for visible wavelengths, i.e., tetradymites and gallium telluride.[22]

The high $k$ modes accessible in multilayer metal−dielectric HMMs are essentially due to the presence of surface plasmon polaritons (SPPs) at each of the metal−dielectric interfaces.[15] Due to the multiple SPP branches in the dispersion characteristics of such HMMs, significant enhancement of the LDOS can then be achieved across a broad spectral region (see Figure S9).[5c] The negative real part of the in-plane complex dielectric function evidenced in QQT(CN)4 films implies the creation of surface polaritonic species.[16] SPPs[17] and surface phonon polaritons[18] can be excluded to explain this result because of the nonmetallic nature and the spectral region of the hyperbolic dispersion of QQT(CN)4 films, respectively. However, previous studies have reported the existence of SEPs[19] in organic single crystals such as those made of polymerized diacetylene.[20] In this context, the attenuated total internal reflection (ATR) technique[21] was



DOI: 10.1021/acsphotonics.9b00185
ACS Photonics 2019, 6, 1681−1689

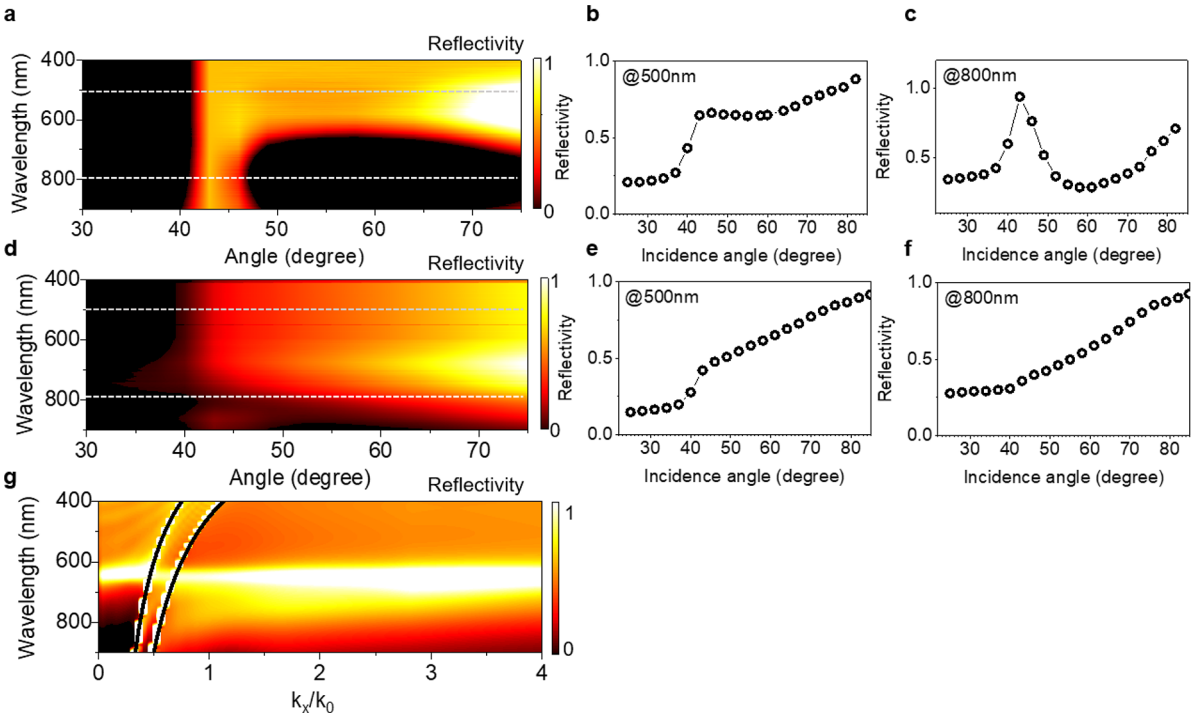


**Figure 2.** (a–c) Measured reflectivity of a QQT(CN)4 neat film as a function of the incidence angle for p-polarized light. (d–f) Measured reflectivity of a QQT(CN)4 neat film as a function of incidence angle for s-polarized light. (g) FDTD-calculated LDOS (normalized dissipated power spectrum of dipoles located inside the natural molecular hyperbolic material) of a QQT(CN)4 film. Black curves indicate the light line in air and glass.

employed to clarify if QQT(CN)4 films can support the presence of SEPs. Details about our experimental setup are provided in the Supporting Information. The ATR sample consisted of a QQT(CN)4 film spin-coated on top of a fused silica substrate, which was then assembled with a coupling prism in the Kretschmann geometry. In this ATR experiment, we measure the reflectivity as a function of the incident angle. In fact, this technique involves the coupling of SEPs to the evanescent electromagnetic field that is present upon total internal reflection of a light beam at a surface in QQT(CN)4 films. Under the resonant conditions for which the in-plane component of the photon wavevector in the prism matches with the SEP wavevector at the QQT(CN)4 film surface, light is coupled to SEPs and a sharp minimum can be seen in the reflectivity from the prism interface. Figure 2a–f show the p-polarized and s-polarized reflectivity of a QQT(CN)4 film as a function of incidence angle and wavelength. The experimental data are in good agreement with the theoretical results (Figure S10) obtained by finite-difference time domain (FDTD) simulations taking into account the Fresnel equations. While both p- and s-polarization have been measured, a reflectivity dip can be seen for wavelengths in the range between 700 and 900 nm only for the p-polarization. This dip lies in the same spectral region as that of the hyperbolic dispersion and demonstrates the existence of SEPs in the QQT(CN)4 films. This study provides evidence of a negative real permittivity supporting SEPs in organic thin films. Obviously, the lamellar crystalline structure of the QQT(CN)4 films plays a crucial role to obtain a strong optical anisotropy and to support a collective coherent oscillation of excitons in each molecular lamella. It is worth noting that the beam size for our ATR measurements was around 400 $\mu$m in diameter, which is several orders of magnitude larger than the average size of the crystallites in QQT(CN)4 films. It should also be mentioned that the ATR response was the same for different locations of the same QQT(CN)4 film. Because all the QQT(CN)4 crystallites in the spin-coated films exhibit a lamellar structure with the lamellae parallel to the substrate plane, the fact that the ATR measurements probe the response from a large number of crystallites is not an issue for the present study. Other aspects should be examined in further investigations such as the role of the oscillator strength of the chromophore and the biradicaloid nature[22] of quinoidal oligothiophenes such as QQT(CN)4 on the epsilon near zero (ENZ) properties.

The hyperbolic dispersion and the existence of SEPs in QQT(CN)4 films should have strong effects on the LDOS and, as a consequence of Fermi's golden rule, on the spontaneous emission rate of emitting dipoles placed inside or nearby the organic monolithic natural hyperbolic material. In that context, we first calculated the LDOS by FDTD simulations in a 60 nm thick QQT(CN)4 film. Figure 2g shows the normalized dissipated power spectrum of dipoles located inside the natural molecular hyperbolic material. The result clearly indicates the presence of additional locally available photon states in the 670 and 920 nm spectral range where QQT(CN)4 films show a hyperbolic dispersion. This enhancement of the LDOS arises from SEP excitations taking place at each interface between quinoidal quaterthiophene-based and insulating alkyl chain based lamellae. At those interfaces, polariton light–matter interaction can be sustained by collective oscillations of excitons in the quinoidal quaterthiophene lamella, giving rise to an optical field confinement at the interfaces. As a consequence of the enhancement of the LDOS by the organic monolithic natural hyperbolic material, tailoring the Purcell factor and the


DOI: 10.1021/acsphotonics.9b00185
ACS Photonics 2019, 6, 1681–1689

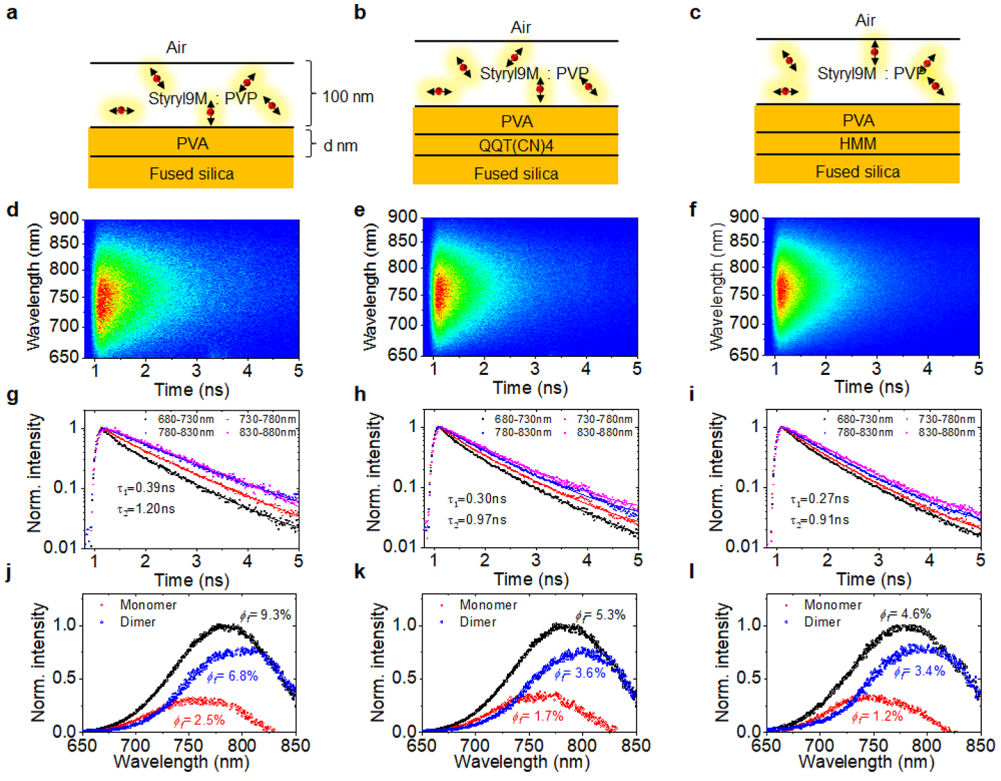


**Figure 3.** Schematic representation of blend films containing a polyvinylpyrrolidone (PVP) host doped with the Styryl9M dye on top of three different types of substrates: (a) fused silica (FS), (b) 60 nm thick QQT(CN)4 films, (c) 80 nm thick dielectric−metal HMMs containing 4 Ag/$Al_2O_3$ pairs. (d−f) Streak camera images, (g−i) PL decays, and (j−l) time-integrated PL spectra together with the emission spectra of the monomeric (with short lifetime $\tau_1$) and dimeric species (with long lifetime $\tau_2$) of Styryl9M on top of FS, QQT(CN)4, and HMM substrates.

photophysical properties of a light-emitting dye located nearby should be possible.

To characterize the influence of QQT(CN)4 hyperbolic films on the photophysical properties of an emitting dye, we prepared blend films containing a polyvinylpyrrolidone (PVP) host doped with the Styryl9M light-emitting dye on top of three different types of substrates: (1) fused silica (FS), (2) 80 nm thick dielectric−metal HMMs containing 4 Ag/$Al_2O_3$ pairs (showing a transverse negative HD),[23] and (3) organic monolithic natural hyperbolic materials based on a 60 nm thick QQT(CN)4 film (see the experimental section for the sample preparation). To gain further insights, poly(vinyl alcohol) (PVA) layers (spin-coated from water) with thicknesses of 25 and 100 nm were also inserted between the three types of substrates and the PVP blends. A schematic representation of the different sample architectures is provided in Figure 3a−c. Despite its rather low PLQY, the styryl9M dye was selected because its 680 to 850 nm emission lies in the 670 to 920 nm hyperbolic spectral range of the QQT(CN)4 thin film and because of its solubility in ethanol. It is also important to note that QQT(CN)4 is insoluble in water and ethanol, allowing to spin-coat PVP and PVA films on top of the QQT(CN)4 layers without any degradation.

Figure S11 displays the steady-state photoluminescence (SSPL) spectra of Styryl9M on top of the QQT(CN)4 samples. It can be seen that the organic monolithic natural hyperbolic material does not significantly affect the emission spectrum. PLQY measurements were carried out in all samples using an integration sphere, correcting for the light absorbed by the metasurfaces (see Supporting Information), and their values are summarized in Table S1. These data reveal a quenching of the emission of the dye when comparing the values on QQT(CN)4 with the one on FS. For instance, in the QQT(CN)4 sample without a spacing layer, PLQY is found to be 5.3%, which is lower than the value of 9.3% measured on the FS substrate. In other words, the spontaneous emission near the QQT(CN)4 film is quenched due to more effective nonradiative decay channels.

Streak camera images and representative spontaneous emission decays of the FS samples are displayed in Figure S12. Similar measurements were carried out in the QQT-(CN)4 samples without and with spacers, and the results are shown in Figure 3d,e,h and Figure S13 respectively. As shown in Figure 3g−l, the photoluminescence decays exhibit an emission wavelength dependence characterized by slower dynamics at longer wavelengths. In addition, a sum of two exponential decay functions was necessary to describe these fluorescence decays. Here, it can be noted the presence of the two fluorescence lifetimes are not due to the anisotropy of the QQT(CN)4 that would result in different effects following *x*,*y* and *z* axis because such an effect would result in spectra with the same energies. Instead, such a behavior was observed in all samples and is attributed to the presence of Styryl9M monomers and higher aggregates in the PVP blends.[24] By using the short-lived emission spectrum of the monomer (monomer, M, $\tau_1$), the spectra of the monomeric and aggregated species (dimer, D, $\tau_2$) can be straightforwardly deconvoluted from the streak camera data. All the measured spontaneous emission lifetimes are listed in Table S1. Noticeably, the faster decays observed in QQT(CN)4 samples are consistent with their lower PLQY values and the quenching of the dye emission by the substrates with hyperbolic



DOI: 10.1021/acsphotonics.9b00185
ACS Photonics 2019, 6, 1681−1689

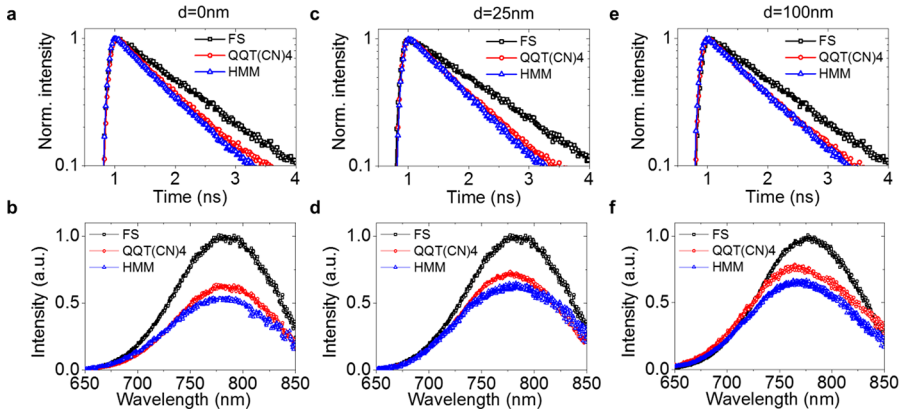


**Figure 4.** (a, c, e) Transient PL decays and (b, d, f) time-integrated PL spectra of Styryl9M on top of fused silica (black dots), QQT(CN)4 (red dots), and HMM (blue dots). Each type of sample has three different spacer thicknesses: (a, b) $d$ = 0 nm, (c, d) $d$ = 25 nm, (e, f) $d$ = 100 nm.

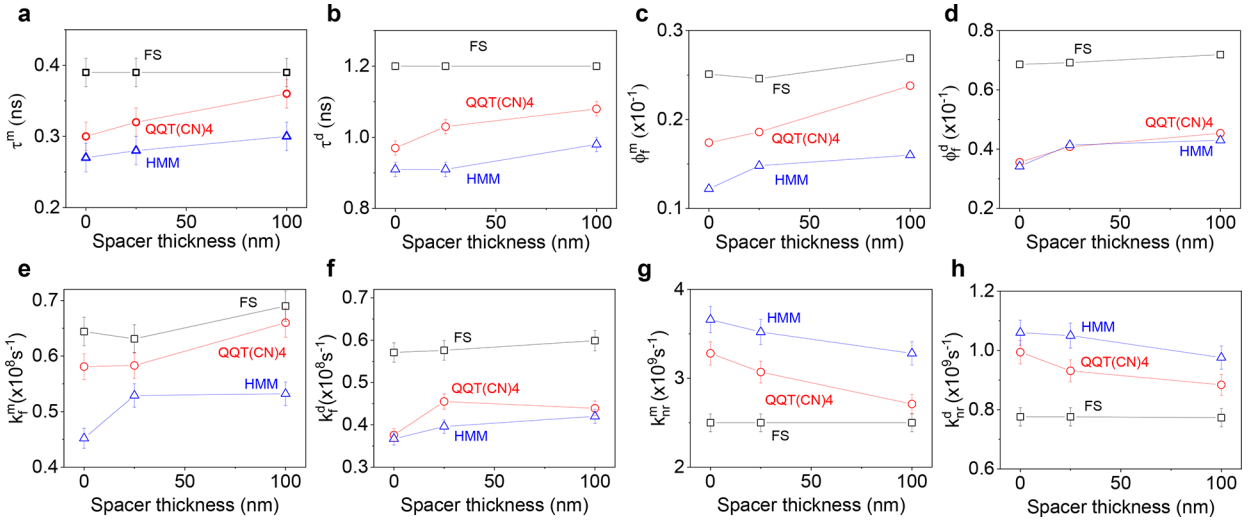


**Figure 5.** (a, b) Measured spontaneous emission lifetime of Styryl9M on top of fused silica (black dots), QQT(CN)4 (red dots), and HMM (blue dots) for (a) monomeric species $\tau^m$ and (b) dimeric species $\tau^d$. (c, d) Measured PLQY ($\phi_f = k_f/k = \tau_f/\tau$) of Styryl9M on top of fused silica (black dots), QQT(CN)4 (red dots), and HMM (blue dots) for (c) monomeric species and (d) dimeric species. (e, f) Radiative decay rate $k_f = \phi_f/\tau_f$ for (e) monomeric and (f) dimeric species. (g, h) Nonradiative decay rate $k_{nr} = (k_f/\phi_f) - k_f$ for (g) monomeric and (h) dimeric species.

dispersion. As shown in Figure 3f,i,l, Figure S14, Figure 4, and Table S1, similar effects on both PLQYs and PL decays were observed in HMM samples.

To gain further insights, we then measured the Purcell factor as well as the radiative and nonradiative decay rates in all QQT(CN)4 samples. The radiative and nonradiative decay rates, noted $k_f$ and $k_{nr}$, respectively, were evaluated using the equations $k_f$ = PLQY/$\tau$ and $k_{nr} = (k_f/\text{PLQY}) - k_f$. The Purcell factor[25] corresponds to the ratio between the decay rate of the emitter placed nearby the QQT(CN)4 substrates and its rate on top of FS substrates. Since Förster energy transfer from the monomer to the aggregates has been identified in similar emitters dispersed into organic matrices,[24a] only $k_f$ and $k_{nr}$ from the lower energy emission are further discussed.[23] Here, it can be noted that we used a PVA spacer (with thicknesses of 25 and 100 nm) in order to exclude energy- and electron-transfer processes between the Styryl9M and QQT(CN)4 layers as quenching mechanism. Since the same effect on the photophysical properties of the light-emitting dye is observed with and without the spacer, such quenching mechanisms can therefore be excluded to explain our results. All the calculated $k_f$ and $k_{nr}$ values are provided in Table S1, and a representative evolution of those parameters are plotted as a function of the spacing distance in Figure 5. Noticeably, the QQT(CN)4 samples display smaller $k_f$ and larger $k_{nr}$ than those measured on FS. It can also be seen that $k_{nr}$ decreases while $k_f$ increases as the spacing distance increases when comparing to the sample on FS (see Figure 5c,d,g,h). The observed behavior of $k_{nr}$ supports our claim regarding the substantial emission quenching by the substrates with hyperbolic dispersion. Interestingly, the results also indicate significant changes in $k_f$,[3a] which can be attributed to the high $k$ states available in media with hyperbolic dispersion. To evaluate and be able to compare the performance of the QQT(CN)4 samples with other systems in terms of spontaneous emission engineering, the measured and calculated Purcell factors (Figure S15) are also plotted as a function of the spacing distance. The Purcell factor is measured to be around 1.3 and 1.4 on top of the QQT(CN)4 and HMM substrates with no spacing layer. For a 100 nm spacing distance, this value decreases to 1.15 and 1.3 for the natural organic hyperbolic material and the HMM, respectively, which can be explained by the hyperbolic dispersion of the substrates and its nonlocal effect[23] on the photophysical properties of the emitter. In addition, it should



DOI: 10.1021/acsphotonics.9b00185
ACS Photonics 2019, 6, 1681−1689

be emphasized that the experimental values of the Purcell factor are in excellent agreement with the calculated values based on FDTD simulations. Such low Purcell factor can be explained by the value of the real part of the dielectric constant, which is less negative when compared with other HMMs. This results in a low quality factor for the Purcell factor, even though QQT(CN)4 has a low imaginary index. The fact that experimental and calculated results obtained on top of a conventional HMM and a QQT(CN)4 film show nearly the same distance dependence and similar absolute values of the Purcell factor undoubtedly provides evidence that hyperbolic modes are involved in the changes of the LDOS and the tailoring of the Purcell factor by the organic natural hyperbolic material.

Previous studies[13b,26] have shown that, when located in the proximity of a multilayer HMM such as the ones used in the present study, light-emitting dipoles release their energy predominantly into three channels: radiative emission, plasmonic modes, and other nonradiative decay channels. In those systems, plasmonic modes usually dominate over the other decay channels. Since HMMs provide a large plasmonic density of states, this leads to an enhancement of the spontaneous emission rate. However, a large part of the emission in the near field goes into high $k$ states and cannot reach the far field. In other words, the nonradiative nature of the dominating plasmonic modes in multilayer HMMs generally leads to a lower PLQY in the far field. Therefore, a variety of schemes[4c,5a,b] have been adopted to out-couple the high $k$ modes to the free space as a far field in order to extract energy more effectively from these nonradiative modes. For instance, Lu et al.[4c] have shown that the spontaneous emission rate of a light-emitting dye can be greatly enhanced by 76-fold enhancement of the Purcell factor, and the emission intensity is enhanced by 80-fold by nanostructuring multilayer HMMs, when compared to HMMs without nanostructuring. Our experimental results with multilayer HMMs are fully consistent with what has been previously reported in the literature. As shown in Figure 4 and Figure 5 as well as in Table S1, we observed a decrease of PLQY for emitters placed nearby the HMM. At the same time, the PL lifetimes are found to be significantly shorter on top of the HMM compared to those measured on top of fused silica. As shown in Figure S15, the Purcell enhancement is observed in the case of HMM samples driven by the local field enhancement resulting from the high $k$ modes that HMMs provide at the location of the light-emitting dipoles. In other words, we observe the lifetime shortening associated with the Purcell factor enhancement at the location of light-emitting dipole by HMMs, mainly from the high $k$ modes which cannot reach the far-field and consequently resulting in a lower PLQY. As shown by the experimental results in Figures 5 and S15 as well as in Table S1, the use of QQT(CN)4 film substrates leads to lower PLQY and a shortening of the PL lifetime of the light-emitting molecules placed nearby. This is exactly the same behavior as that observed when the emitters are located near a multilayer HMM. We can see however that the changes in PLQY and PL lifetimes are smaller in the case of QQT(CN)4 samples than for the HMMs. This can be understood by the fact that, compared to conventional multilayer HMM, the organic hyperbolic material has a larger portion of low $k$ modes which can reach the far field and do not contribute to the PL lifetime shortening. This latter statement is supported by the calculations of the LDOS of the natural organic hyperbolic material in Figure 2 and the multilayer HMM in Figure S9. Overall, this study demonstrates that the accessible high $k$ modes due to the presence of an organic natural hyperbolic material lead to changes in the spontaneous emission decay rate and PLQY of light-emitting molecules placed nearby.

These photophysical results demonstrate that the observed changes in PLQYs, spontaneous emission decay rates, and Purcell factors are due to the effects of HMM and QQT(CN)4 substrates on both radiative and nonradiative decay processes when compared to FS. The effective nonradiative decay processes in HMM samples are due to the efficient quenching of the emission by SPPs and the larger number of accessible high $k$ modes. Regarding the QQT(CN)4 samples, quenching of the emission of the dye is due to the hyperbolic dispersion caused by SEPs. Since the effect is observed in samples containing a PVA spacer, electron transfer and/or energy transfer involving QQT(CN)4 as an acceptor can be excluded. We therefore attribute the enhancement of the nonradiative decay channels to the coupling of the radiative waves with the SEP modes, which noticeably is also the first experimental demonstration of the SEP effect on emitters. The comparison of the photophysical properties in the samples used in this study demonstrates that the organic monolithic natural hyperbolic material, similarly to conventional metal−dielectric multilayer HMMs, is able to control the spontaneous emission decay rate of an emitter. These results show that natural molecular hyperbolic materials represent a promising alternative for tailoring the Purcell factor of any emitter in the visible and near-infrared region upon engineering the chemical structure of the organic molecules. Therefore, natural molecular hyperbolic materials are shown to be promising systems for device applications requiring an effective emission decay rate control. In addition, it should be emphasized that all the QQT(CN)4 films for the ATR and photophysical measurements were prepared in an ambient atmosphere by spin-coating onto substrates with a size of 2 × 2 $cm^2$. Considering the fact that their optical and photophysical properties were found to be the same for different locations of the same QQT(CN)4 film, this supports the conclusion that organic natural hyperbolic materials can be prepared onto a large area by a simple and low-cost technique such as spin-coating, making these systems particularly promising for a next generation of photonic applications.

In conclusion, we demonstrate that organic monolithic natural hyperbolic materials can provide an unprecedented flexible platform for the control of the radiative emission over a wide spectral range in the visible/NIR region. Similarly to HMMs, the PLQY and spontaneous emission decay rate of an emitter placed nearby the organic monolithic natural hyperbolic material are modified by changes in both radiative and nonradiative decay rates. In the case of organic materials, tailoring the Purcell factor is possible due to changes of the LDOS associated with the presence of SEPs in the layered molecular crystalline structure. These important results open a new route toward a next generation of metal-free materials with hyperbolic dispersion in the visible/NIR spectral range. It should be emphasized that organic monolithic natural hyperbolic materials present several remarkable advantages compared to conventional artificial HMMs, including their low-cost and simple processing, their compatibility with the fabrication of lightweight and large-area photonic devices, and their mechanical flexibility. More importantly, the possibility to achieve a hyperbolic dispersion in organic semiconducting thin



DOI: 10.1021/acsphotonics.9b00185
ACS Photonics 2019, 6, 1681−1689

films implies that the optical properties of organic monolithic natural hyperbolic materials can be modified by chemical engineering. This provides a large number of exciting opportunities in the near future to develop new molecular systems with improved performances and tunable optical properties.

## ■ ASSOCIATED CONTENT

### Supporting Information

The Supporting Information is available free of charge on the ACS Publications website at DOI: 10.1021/acsphotonics.9b00185.

Experimental details, characterization of the optical properties of the QQT(CN)4 films, complex permittivities and LDOS of HMMs, calculated ATR curves of QQT(CN)4 films, influence of the QQT(CN)4 and HMM substrates on the photophysical properties of a light-emitting dye (PDF)

## ■ AUTHOR INFORMATION


### Corresponding Authors

*E-mail: jwwu@ewha.ac.kr.
*E-mail: anthony.daleo@cnrs.fr.
*E-mail: ribierre@opera.kyushu-u.ac.jp.

### ORCID

Kazuto Takaishi: 0000-0003-4979-7375
Pascal André: 0000-0001-9334-5638
Atsuya Muranaka: 0000-0002-3246-6003
Jean-Charles Ribierre: 0000-0001-7288-3795


### Notes

The authors declare no competing financial interest.

## ■ ACKNOWLEDGMENTS

J.C.R. and P.A. would like to acknowledge funding from the Royal Society (International Joint Project ref. JP0869934). P.A. would like to thank the Canon Foundation in Europe for supporting his Fellowship. This work was carried out in the framework of CNRSUMI2002 2B-FUEL "Building Blocks for Future Electronics Laboratory" and CNRS International Associated Laboratory "Functional Nanostructures: Morphology, Nanoelectronics and Ultrafast Optics" (LIA NANOFUNC) and was supported by funding of the Ministry of Science, ICT & Future Planning, Korea (2014M3A6B3063708, 2017R1E1A1A01075394). J.C.R. acknowledges financial support from the National Natural Science Foundation of China (61874096).

## ■ REFERENCES


(1) (a) Poddubny, A.; Iorsh, I.; Belov, P.; Kivshar, Y. Hyperbolic metamaterials. *Nat. Photonics* **2013**, *7* (12), 948−957. (b) Noginov, M.; Lapine, M.; Podolskiy, V.; Kivshar, Y. Focus issue: hyperbolic metamaterials. *Opt. Express* **2013**, *21* (12), 14895−14897.

(2) (a) Yao, J.; Liu, Z.; Liu, Y.; Wang, Y.; Sun, C.; Bartal, G.; Stacy, A. M.; Zhang, X. Optical Negative Refraction in Bulk Metamaterials of Nanowires. *Science* **2008**, *321* (5891), 930. (b) Shalaev, V. M. Optical negative-index metamaterials. *Nat. Photonics* **2007**, *1* (1), 41−48. (c) Jacob, Z.; Alekseyev, L. V.; Narimanov, E. Optical Hyperlens: Far-field imaging beyond the diffraction limit. *Opt. Express* **2006**, *14* (18), 8247−8256. (d) Liu, Z.; Lee, H.; Xiong, Y.; Sun, C.; Zhang, X. Far-Field Optical Hyperlens Magnifying Sub-Diffraction-Limited Objects. *Science* **2007**, *315* (5819), 1686.

(3) (a) Barnes, W. L. Fluorescence near interfaces: The role of photonic mode density. *J. Mod. Opt.* **1998**, *45* (4), 661−699. (b) Jacob, Z.; Kim, J. Y.; Naik, G. V.; Boltasseva, A.; Narimanov, E. E.; Shalaev, V. M. Engineering photonic density of states using metamaterials. *Appl. Phys. B: Lasers Opt.* **2010**, *100* (1), 215−218. (c) Iorsh, I.; Poddubny, A.; Orlov, A.; Belov, P.; Kivshar, Y. S. Spontaneous emission enhancement in metal−dielectric metamaterials. *Phys. Lett. A* **2012**, *376* (3), 185−187.

(4) (a) Jacob, Z.; Smolyaninov, I. I.; Narimanov, E. E. Broadband Purcell effect: Radiative decay engineering with metamaterials. *Appl. Phys. Lett.* **2012**, *100* (18), 181105. (b) Noginov, M. A.; Li, H.; Barnakov, Y. A.; Dryden, D.; Nataraj, G.; Zhu, G.; Bonner, C. E.; Mayy, M.; Jacob, Z.; Narimanov, E. E. Controlling spontaneous emission with metamaterials. *Opt. Lett.* **2010**, *35* (11), 1863−1865. (c) Lu, D.; Kan, J. J.; Fullerton, E. E.; Liu, Z. Enhancing spontaneous emission rates of molecules using nanopatterned multilayer hyperbolic metamaterials. *Nat. Nanotechnol.* **2014**, *9* (1), 48−53.

(5) (a) Kabashin, A. V.; Evans, P.; Pastkovsky, S.; Hendren, W.; Wurtz, G. A.; Atkinson, R.; Pollard, R.; Podolskiy, V. A.; Zayats, A. V. Plasmonic nanorod metamaterials for biosensing. *Nat. Mater.* **2009**, *8* (11), 867−871. (b) Esfandyarpour, M.; Garnett, E. C.; Cui, Y.; McGehee, M. D.; Brongersma, M. L. Metamaterial mirrors in optoelectronic devices. *Nat. Nanotechnol.* **2014**, *9* (7), 542−547. (c) Boriskina, S. V.; Ghasemi, H.; Chen, G. Plasmonic materials for energy: From physics to applications. *Mater. Today* **2013**, *16* (10), 375−386.

(6) (a) Boltasseva, A.; Atwater, H. A. Low-Loss Plasmonic Metamaterials. *Science* **2011**, *331* (6015), 290. (b) West, P. R.; Ishii, S.; Naik, G. V.; Emani, N. K.; Shalaev, V. M.; Boltasseva, A. Searching for better plasmonic materials. *Laser Photon. Rev.* **2010**, *4* (6), 795−808.

(7) (a) Li, P.; Lewin, M.; Kretinin, A. V.; Caldwell, J. D.; Novoselov, K. S.; Taniguchi, T.; Watanabe, K.; Gaussmann, F.; Taubner, T. Hyperbolic phonon-polaritons in boron nitride for near-field optical imaging and focusing. *Nat. Commun.* **2015**, *6*, 7507. (b) Caldwell, J. D.; Kretinin, A. V.; Chen, Y.; Giannini, V.; Fogler, M. M.; Francescato, Y.; Ellis, C. T.; Tischler, J. G.; Woods, C. R.; Giles, A. J.; Hong, M.; Watanabe, K.; Taniguchi, T.; Maier, S. A.; Novoselov, K. S. Sub-diffractional volume-confined polaritons in the natural hyperbolic material hexagonal boron nitride. *Nat. Commun.* **2014**, *5*, 5221. (c) Narimanov, E. E.; Kildishev, A. V. Metamaterials: Naturally hyperbolic. *Nat. Photonics* **2015**, *9* (4), 214−216.

(8) Esslinger, M.; Vogelgesang, R.; Talebi, N.; Khunsin, W.; Gehring, P.; de Zuani, S.; Gompf, B.; Kern, K. Tetradymites as Natural Hyperbolic Materials for the Near-Infrared to Visible. *ACS Photonics* **2014**, *1* (12), 1285−1289.

(9) Gjerding, M. N.; Petersen, R.; Pedersen, T. G.; Mortensen, N. A.; Thygesen, K. S. Layered van der Waals crystals with hyperbolic light dispersion. *Nat. Commun.* **2017**, *8* (1), 320.

(10) Handa, S.; Miyazaki, E.; Takimiya, K.; Kunugi, Y. Solution-Processible n-Channel Organic Field-Effect Transistors Based on Dicyanomethylene-Substituted Terthienoquinoid Derivative. *J. Am. Chem. Soc.* **2007**, *129* (38), 11684−11685.

(11) Kim, R. H.; Kim, H. J.; Bae, I.; Hwang, S. K.; Velusamy, D. B.; Cho, S. M.; Takaishi, K.; Muto, T.; Hashizume, D.; Uchiyama, M.; André, P.; Mathevet, F.; Heinrich, B.; Aoyama, T.; Kim, D.-E.; Lee, H.; Ribierre, J.-C.; Park, C. Non-volatile organic memory with sub-millimetre bending radius. *Nat. Commun.* **2014**, *5*, 3583.

(12) Ribierre, J.-C.; Watanabe, S.; Matsumoto, M.; Muto, T.; Nakao, A.; Aoyama, T. Reversible Conversion of the Majority Carrier Type in Solution-Processed Ambipolar Quinoidal Oligothiophene Thin Films. *Adv. Mater.* **2010**, *22* (36), 4044−4048.

(13) (a) Shin, H. Y.; Woo, J. H.; Gwon, M. J.; Barthelemy, M.; Vomir, M.; Muto, T.; Takaishi, K.; Uchiyama, M.; Hashizume, D.; Aoyama, T.; Kim, D. W.; Yoon, S.; Bigot, J. Y.; Wu, J. W.; Ribierre, J. C. Exciton diffusion in near-infrared absorbing solution-processed organic thin films. *Phys. Chem. Chem. Phys.* **2013**, *15* (8), 2867−2872. (b) Ribierre, J. C.; Yokota, Y.; Sato, M.; Ishizuka, A.; Tanaka, T.; Watanabe, S.; Matsumoto, M.; Muranaka, A.; Matsumoto, S.;




DOI: 10.1021/acsphotonics.9b00185
*ACS Photonics* 2019, 6, 1681−1689

Uchiyama, M.; Aoyama, T. Influence of the grain orientation on the charge transport properties of organic field-effect transistors. *RSC Adv.* **2014**, *4* (69), 36729−36737.
(14) Janzen, D. E.; Burand, M. W.; Ewbank, P. C.; Pappenfus, T. M.; Higuchi, H.; da Silva Filho, D. A.; Young, V. G.; Brédas, J.-L.; Mann, K. R. Preparation and Characterization of π-Stacking Quinodimethane Oligothiophenes. Predicting Semiconductor Behavior and Bandwidths from Crystal Structures and Molecular Orbital Calculations. *J. Am. Chem. Soc.* **2004**, *126* (46), 15295−15308.
(15) Zhukovsky, S. V.; Kidwai, O.; Sipe, J. E. Physical nature of volume plasmon polaritons in hyperbolic metamaterials. *Opt. Express* **2013**, *21* (12), 14982−14987.
(16) (a) Low, T.; Chaves, A.; Caldwell, J. D.; Kumar, A.; Fang, N. X.; Avouris, P.; Heinz, T. F.; Guinea, F.; Martin-Moreno, L.; Koppens, F. Polaritons in layered two-dimensional materials. *Nat. Mater.* **2017**, *16* (2), 182−194. (b) Basov, D. N.; Fogler, M. M.; García de Abajo, F. J., Polaritons in van der Waals materials. *Science* **2016**, *354* (6309), aag1992.
(17) Barnes, W. L.; Dereux, A.; Ebbesen, T. W. Surface plasmon subwavelength optics. *Nature* **2003**, *424* (6950), 824−830.
(18) Ocelic, N.; Hillenbrand, R. Subwavelength-scale tailoring of surface phonon polaritons by focused ion-beam implantation. *Nat. Mater.* **2004**, *3* (9), 606−609.
(19) (a) Lagois, J.; Fischer, B. Experimental Observation of Surface Exciton Polaritons. *Phys. Rev. Lett.* **1976**, *36* (12), 680−683. (b) Lagois, J.; Fischer, B. Dispersion theory of surface-exciton polaritons. *Phys. Rev. B: Condens. Matter Mater. Phys.* **1978**, *17* (10), 3814−3824.
(20) Brillante, A.; Pockrand, I.; Philpott, M. R.; Swalen, J. D. Experimental observation of exciton surface polaritons on a polymerized diacetylene crystal. *Chem. Phys. Lett.* **1978**, *57* (3), 395−399.
(21) (a) Seshadri, S. R. Attenuated total reflection method of excitation of the surface polariton in the Kretschmann configuration. *J. Appl. Phys.* **1991**, *70* (7), 3647−3654. (b) Philpott, M. R.; Pockrand, I.; Brillante, A.; Swalen, J. D. Experimental and theoretical study of exciton surface polaritons on organic crystals. II. Highly reflecting faces of CTIP and PTS. *J. Chem. Phys.* **1980**, *72* (4), 2774−2787. (c) Dickson, W.; Beckett, S.; McClatchey, C.; Murphy, A.; O'Connor, D.; Wurtz, G. A.; Pollard, R.; Zayats, A. V. Hyperbolic polaritonic crystals based on nanostructured nanorod metamaterials. *Adv. Mater.* **2015**, *27*, 5974−5980.
(22) Ponce Ortiz, R.; Casado, J.; Hernández, V.; López Navarrete, J. T.; Viruela, P. M.; Ortí, E.; Takimiya, K.; Otsubo, T. On the Biradicaloid Nature of Long Quinoidal Oligothiophenes: Experimental Evidence Guided by Theoretical Studies. *Angew. Chem., Int. Ed.* **2007**, *46* (47), 9057−9061.
(23) Lee, K. J.; Lee, Y. U.; Fages, F.; Ribierre, J.-C.; Wu, J. W.; D'Aléo, A. Blue-Shifting Intramolecular Charge Transfer Emission by Nonlocal Effect of Hyperbolic Metamaterials. *Nano Lett.* **2018**, *18* (2), 1476−1482.
(24) (a) D'Aléo, A.; Sazzad, M. H.; Kim, D. H.; Choi, E. Y.; Wu, J. W.; Canard, G.; Fages, F.; Ribierre, J. C.; Adachi, C. Boron difluoride hemicurcuminoid as an efficient far red to near-infrared emitter: toward OLEDs and laser dyes. *Chem. Commun.* **2017**, *53* (52), 7003−7006. (b) Kim, D.-H.; D'Aléo, A.; Chen, X.; Sandanayaka, A. S. D.; Yao, D.; Zhao, L.; Komino, T.; Zaborova, E.; Canard, G.; Tsuchiya, Y.; Choi, E.; Wu, J. W.; Fages, F.; Brédas, J.-L.; Ribierre, J.-C.; Adachi, C. High-efficiency electroluminescence and amplified spontaneous emission from a thermally-activated delayed fluorescent near infrared emitter. *Nat. Photonics* **2018**, *12*, 98−104.
(25) Purcell, E. M. Spontaneous Emission Probabilities at Radio Frequencies. In *Confined Electrons and Photons: New Physics and Applications*; Burstein, E.; Weisbuch, C., Eds.; Springer US: Boston, MA, 1995; pp 839−839.
(26) Cornil, J.; Calbert, J. P.; Beljonne, D.; Silbey, R.; Brédas, J. L. Charge Transport versus Optical Properties in Semiconducting Crystalline Organic Thin Films. *Adv. Mater.* **2000**, *12* (13), 978−983.



DOI: 10.1021/acsphotonics.9b00185
*ACS Photonics* 2019, 6, 1681−1689